We are IntechOpen,
the world's leading publisher of
Open Access books
Built by scientists, for scientists

6,900
Open access books available

186,000
International authors and editors

200M
Downloads

154
Countries delivered to

Our authors are among the

TOP 1%
most cited scientists

12.2%
Contributors from top 500 universities

BOOK CITATION INDEX CLARIVATE ANALYTICS INDEXED

WEB OF SCIENCE™

Selection of our books indexed in the Book Citation Index
in Web of Science™ Core Collection (BKCI)

Interested in publishing with us?
Contact book.department@intechopen.com

Numbers displayed above are based on latest data collected.
For more information visit www.intechopen.com

Preparation and Characterization of Fe$_2$O$_3$-SiO$_2$ Nanocomposite for Biomedical Application

Violeta N. Nikolić

Abstract

The scope of this chapter is to get deeper insight into the correlation between synthesis parameters and magnetic behavior of the nanocomposite materials containing hematite (α-Fe$_2$O$_3$) nanoparticles. Potential applications of nano-hematite in biomedicine are listed in the short overview. Then, basic requirements necessary for synthesis of high-quality nanoparticles for biomedical application are summarized. The next part of the chapter is devoted to the sol-gel synthesis that is recognized as suitable for preparation of the nanocomposite materials containing α-Fe$_2$O$_3$ nanoparticles. Having in mind that sol-gel method considers preparation of hematite nanoparticles via Fe$_2$O$_3$ phase transformations initiated by thermal treatment at high temperatures, coexistence of the other iron oxides (such as ε-Fe$_2$O$_3$) with α-Fe$_2$O$_3$ phase is commented. Special attention is paid on mechanism of the critical field (which is in literature usually denoted as coercivity field) alterations. Diffraction patterns and hysteresis measurements of the chosen samples containing hematite nanoparticles in the silica matrix are represented. Finally, variations in the observed measured critical field values are discussed.

Keywords: nano α-Fe$_2$O$_3$-phase, nano ε-Fe$_2$O$_3$-phase, silica, synthesis parameters, intrinsic coercivity field, biomedical application

1. Introduction

Hematite (α-Fe$_2$O$_3$) has been thoroughly investigated during the centuries, since it is one of the most abundant minerals in the earth's crust: on the surface as well as at the bottom of the sea [1, 2]. From the beginning of its discovery to the present days, α-Fe$_2$O$_3$ gained attention of the scientific community due to its magneto-structural properties, high resistance to corrosion, easy accessibility, wide distribution in natural environment, and biocompatibility. Accordingly, α-Fe$_2$O$_3$ is recognized as a material of significance in different scientific areas [3–12].

The usage of hematite in conventional biomedicine has been enabled by the breakthrough and development of the nanoscience. Progress in this field is achieved by detailed research of iron oxide polymorphs' physical and chemical properties on the nanoscale. Properties of nm-sized particles are significantly differed from their bulk counterparts due to various nano-size-related effects, appeared as a consequence of the changed ratio of surface and volume atoms. Approaching nanometer dimensions, the ratio of the surface atoms in the overall nanoparticle volume

drastically increased by decreasing particle size, favoring the role of the surface effects in the characteristic behavior of the nanoparticles.

Although the most attention in this chapter will be paid to magnetic properties of hematite nanoparticles, it is important to mention that overall behavior of nano-hematite is characterized by its electromagnetic response which determined biomedical application of nanoparticles. Due to coupling between nano-hematite electrical and magnetic fields, it is clear that electrical properties are contributing to the final hematite application as well as magnetic properties. Noteworthy, difference between conductivity of bulk and nano-hematite widespread biomedical application of this iron oxide polymorph application. According to the analysis of the density of electronic states, the bulk hematite showed the charge-transfer insulator nature [13]. Differed from bulk hematite, nano-hematite is an n-type semiconductor, with a bandgap of ~2.2 eV [14]. Consequently, the increase in conductivity enables the extended application of nano-hematite in different biomedical areas, such as transfer of electrical signals in biosensors, tissue engineering, neural probes, drug delivery, or diagnosis, and therapy of human diseases [15].

On the other hand, transition from bulk to nano dimensions resulted in the significant change of its magnetic behavior. Magnetic behavior of bulk hematite is determined by Neel temperature (T_N) (~950 K) and Morin temperature (T_M) (~260 K) that represent the temperatures upon which the hematite magnetic ordering is changed. Above T_N, hematite is characterized by paramagnetic structure. In the temperature range between T_N and T_M, hematite showed a weak ferromagnetic ordering, while under T_M it is antiferromagnetic [16]. Hematite magnetic configurations are defined by the magnetic interactions (magnetic ordering of bulk materials is mostly influenced by the exchange interaction) [17].

Magnetic structure of bulk hematite is represented by different regions of a macroscopic system broken symmetry in different ways, the so-called domains. Domains present small regions within each of which the local magnetization achieves the saturation value [17], while interface between the adjacent regions presents the domain wall. The processes of magnetization and demagnetization of materials occurred through the movement of the domain walls and change of the domain boundaries, consequently bringing to the increase/decrease of a domain size.

From the aspect of magnetic interactions, decrease of the particle size revealed a dominant role of dipole-dipole interactions in the ordering of nanoparticles' magnetic moments, which is negligible in the case of bulk hematite, since magnetic moment of bulk magnetic material is significantly lower than the moment of the nanoparticle [17]. To get a better insight in the changes in the strength ratio of bulk and nano-magnetic interactions that are responsible for maintaining of long-term ordering of magnetic moments, it is important to understand the origin of the increase in the value of nanoparticle magnetic moment. The increase of magnetic moment occurred as a consequence of lowering dimensionality of bulk materials and has been explained by the absence of multi-domain structure and appearance of single-domain nanoparticle structure. The balance between the anisotropy and exchange energies is required for formation of finite-size domain walls [18], resulting in the presence of some critical diameter size, below which nanoparticle is single-domain [18], Eq. (1):

$$r_c \approx 9\left[(J_{ab} \cdot K_a)^{1/2}/\mu_o \cdot M_s^2\right] \qquad (1)$$

where J_{ab} is the exchange integral, K_a is the anisotropy constant, and M_s is the saturation magnetization.

Noteworthy, macroscopic magnetic properties of nanoparticles are mostly influenced by Zeeman energy, thermal energy, and anisotropy energy. The relations of mentioned energies [19] enable the appearance of a new magnetic state in nanomaterials, characterized by a presence of single-domain particles—superparamagnetic nanoparticles. The main characteristic of superparamagnetic nanoparticle system is the absence of coercivity and remanence at room temperature, which enables the application of magnetic properties of nano-hematite in biomedicine.

Considering the fact that nanomaterials possesses high surface-to-volume ratio and increased surface activity [11], it is obvious that hematite nanoparticles show various magnetic behavior dependent on the size and shape of the particles [12, 20]. Also, it is important to notice that observation of dependence of magnetic or electric properties of nano-hematite on synthesis conditions is enabled by the change of particle size, carrier density (that is dependent on the particle size), domain size, and structure of the synthesized nanoparticles. Furthermore, alteration of synthesis conditions enabled tailoring of their magneto-structural properties and a variety of new applications.

When we are dealing with potential usage of nano-hematite particles in biomedicine, it should be emphasized that biomedical application requires utilization of nanocomposite materials. For preparation of nanocomposites containing α-Fe$_2$O$_3$ nanoparticles convenient for this purpose, silica is recognized as a suitable material.

In order to get deeper insight in the magnetic behavior of the nanocomposites, samples that contained hematite nanoparticles in silica matrix are often prepared by sol-gel method that involves formation of hematite nanoparticles by the phase transformations of the Fe$_2$O$_3$ polymorph (maghemite (γ-Fe$_2$O$_3$) and epsilon phases (ε-Fe$_2$O$_3$)). Due to the presence of particle size distribution in the nanomaterials, special attention should be addressed to the problem of coexistence of different iron oxide species within the silica matrix.

Usually the goal of the synthesis is the preparation of the samples characterized by high purity, containing only one iron oxide phase. In some cases the usage of precisely one phase of the iron oxide polymorph is not of crucial importance. For example, magnetite and maghemite nanoparticles are characterized by similar magneto-structural properties and thus could be used together for the preparation of the magnetic ferrofluids. Noteworthy, synthesis of the nanocomposite materials containing this type of iron oxide nanoparticles is so common in literature that the scientific community accepted the abbreviation "SPION" (superparamagnetic iron oxide nanoparticles) to describe spinel iron oxide species [21, 22].

Comparing the magnetic behavior of hematite nanoparticles with the magnetic properties of the other iron oxides (spinel or epsilon phase), it is certain that α-Fe$_2$O$_3$ cannot be used together with spinel phases due to very different magnetic properties. On the other side, at the moment it is not possible to claim with certainty whether it could be used together with the epsilon phase or not. This is a consequence of the insufficient knowledge about magnetic properties of these two iron oxide phases. Literature data revealed that pure hematite nanoparticles are characterized by the intrinsic coercivity field (H$_{ci}$) value of 1.7 kOe [23], although nano-sized α-Fe$_2$O$_3$ in silica matrix can achieve coercivity of 4.3 kOe [24]. Under the certain size limit, hematite nanoparticles showed superparamagnetic (SPM) behavior [12]. The presence of the other ions significantly alters hematite coercivity. Even bulk hematite doped with alumina ions reached coercivity of >8 kOe [25]. It is similar with the lack of the knowledge regarding epsilon H$_c$ value: dependent on the synthesis conditions, epsilon nanoparticles showed different coercivity. This phase is characterized by high

room temperature coercivity (10–20 kOe) [26, 27]. Nevertheless, some literature reports depicted the lowered epsilon H_c value (8 or 2.4 kOe [28, 29]). As well, epsilon nanoparticles could be prepared in order to display SPM behavior [30]. Although hematite nanoparticles cannot achieve coercivity of 10–20 kOe, there is a certain interval of H_{ci} values during which the hematite and epsilon phase coercivities could overlap. Likewise, it is important to point out that coercivity of the samples containing both phases, hematite and epsilon, significantly varies dependent on the synthesis conditions.

The aim of this chapter was to examine in more detail the correlation between synthesis parameters and magnetic properties of nanocomposites containing pure hematite phase or hematite phase in combination with the SPM epsilon phase. A better insight in the measured magnetic field (which is in literature usually denoted as coercivity field) variations dependence on the synthesis conditions is of importance for improvement of the current efforts in understanding of the magnetic properties of hematite phase. Also, some difficulties inherent in studying influence of the variation of synthesis conditions onto the magnetic behavior of the examined samples are highlighted. Results summarized in this chapter could facilitate application of nano-hematite in biomedicine.

2. Overview of nano-hematite applications in biomedicine

Plenty of synthesis pathways for production of the nano-hematite enabled formation of hematite nanoparticles characterized by different properties, which determine their application. There are a lot of reasons for a biomedical application of nano-sized α-Fe_2O_3: low cost, long-term chemical stability, and nontoxicity. Up until today, nano-hematite is mostly used as a starting material for preparation of multifunctional nanocomposite particles that found application in different areas of biomedicine. In order to obtain appropriate candidate for biomedical application, nanocomposite materials containing hematite nanoparticles are prepared by a few steps of synthesis procedures.

Some of the biomedical applications of *α-Fe_2O_3* nanoparticles are listed below.

Nano-hematite could be used as a starting material for the synthesis of platforms, presenting promising functional nanomaterials for drug delivery and hyperthermia treatments. Liu et al. synthesized α-Fe_2O_3 nanoparticles by hydrothermal method [31]. Particles were further coated with a nonporous silica (Fe_2O_3@SiO_2) and subsequently treated with an organosilicate-incorporated silica by simultaneous sol-gel polymerization of tetraethoxysilane (TEOS) and n-octadecyltrimethoxysilane (C_{18}TMS). Final step of the synthesis considered reduction of the hematite cores to magnetite. Obtained nanocomposite platforms are used as smart-targeted drug delivery materials for further in vivo evaluation of cancer therapies [31]. Another application of the platforms based on the usage of nano-hematite as a starting material is considered a preparation of asymmetric hematite-silica nanocomposites (JFSNs) as multifunctional peroxidase mimetics that found application in glucose colorimetric biosensing [32].

On the other hand, a combination of mesoporous nano-hematite with carbon quantum dots enabled preparation of the nanomaterial that showed promising properties for the application in visible photo-light photocatalysis [33]. Due to very good photocatalytic properties, excellent biocompatibility, and high chemical stability, carbon quantum dots/mesoporous hematite nanocomposites could be used in numerous biomedical applications, such as photodynamic therapy for cancer treatment, drug delivery systems, cell imaging, biosensors for biological assay, and genetic engineering [34].

Mirzaei et al. investigated the usage of materials consisting nano-hematite in biosensor technologies [35]. Nanocomposite material was prepared by Pechini sol-gel method that involved the formation of a complex between hematite nanoparticles and citric acid, followed by an esterification reaction with ethylene glycol. Since hematite nanoparticles are displaying good electrical and sensing stability, nanocomposite material is used as a highly stable and selective biochemical sensor for detection of ethanol and monitoring alcohol consumption [35, 36]. Another biosensing application of hematite nanoparticles denoted the application of anodization method that enables synthesis of highly ordered hematite nanotube array on a patterned SiO_2/Si substrate. Prepared nanomaterial showed an excellent selectivity and ppb-level detection limits toward acetone, depicting its promising application for breath analyzers to diagnose diabetes mellitus [37]. As well, nano-hematite is recognized as a suitable material for magnetically assisted binding assays (measurement of the concentration or potency of a substance by its effect on living cells or tissues) performed by using magnetically labeled binding members [38].

It is important to notice that SPM hematite nanoparticles also could be utilized for biomedical applications, in fabrication of biomolecular sensor system, used for detection of intravenously introduced nanoparticles. Litvinov showed that α-Fe₂O₃ nanoparticles could be used as magnetoresistive nanosensors designed for sensing biomolecule-conjugated nanoparticles (different targets could be detected, such as cell surface receptor, protein, nucleic acid, mRNA, genomic DNA, etc.) [37].

Recent scientific work on *α-Fe₂O₃* revealed a potential application of hematite nanoparticles in genotyping, since results of scientific investigation confirmed the presence of interaction between appreciably high concentration of hematite nanoparticles and drying pattern of a sessile droplet of genomic deoxyribonucleic acid (DNA) [38].

3. Prerequisite conditions for preparation of high-quality nano-hematite particles

An important step in the usage of materials that contained nano-hematite in biomedical application presents synthesis of high-quality nano-hematite particles and high control of its magnetic behavior. To use hematite nanoparticles in biomedical purposes, it is necessary first to modify the surface of nano-hematite.

The nanoparticle surface presents a key factor that determines biocompatibility and enables cell adhesion of the particle injected in the human body. Accordingly, the surface of the nano-hematite particles, predetermined for biomedical application, has to meet few basic requirements:

1. Biocompatibility: non-toxicity for human organism is prerequisite for the application in biomedicine.

2. Monodispersity: uniform nanoparticle size and shape minimized interparticle interactions and agglomeration. This task is not completely overcome up until today, due to the presence of the particle size and shape distribution. For that reason, different synthesis strategies are employed with the aim to improve the knowledge regarding achieving nanoparticles' monodispersity [39, 40]. Reaching monodispersity would allow improvement of the control of magnetic behavior of the overall sample.

3. Functionalization: particles should possess high efficiency for binding target molecules, and non-specific binding should be avoided. In order to ensure the

listed requirements, hematite nanoparticles for application in biomedicine are coated by biocompatible materials (usually with silica, although different materials, such as dextran or citric acid, also could be applied [41–44]) and then further functionalized by attaching groups on the surface (different antibodies, oligonucleotides, or peptide ligands, depending on the desired application [45–47]) via various chemical methods [48–52]. An alternative way for production of suitable nanocomposites presents performing core-shell strategy or encapsulation of the particles in a silica matrix.

4. Sol-gel synthesis

In order to better examine the magnetic behavior of the hematite nanoparticles that could be used as a starting material for different biomedical applications, nanocomposite materials based on hematite are often prepared by sol-gel method. From the point of view of correlation of the synthesis conditions with characteristics of the investigated nanomaterial, this synthesis method is of great significance.

Advantages of this type of synthesis are low price of the chemicals, gelation process under ambient conditions, as well as possibility of the synthesis of very small nanoparticles (~1 nm) [53]. Basic compounds used in the sol-gel synthesis are iron ion precursor, silica ion precursor (tetraethyl orthosilicate, TEOS, or tetramethyl orthosilicate, TMOS), water, and the compound miscible with (mutually nonmiscible) alkoxide precursor and water (ethanol or methanol, depending on the usage of TEOS or TMOS, respectively).

Mechanism of the sol-gel synthesis contains few stages. The first stage consisted nucleation of the Fe_2O_3 and SiO_2 nanoparticles during the hydrolysis of TEOS. Reactions of condensation and polycondensation occurred during the mixing solution and resulted in the nanoparticle growth through the process of Ostwald ripening [53]. Mentioned processes occur at room temperature, conditioning the usage of catalyst, which initiates the changes in the structure and properties of the resulting material. The aging of the prepared sol enables its conversion into gel, which presents the second important stage, followed by drying of the gel (third stage), and subsequently annealing treatment (fourth stage). During the annealing process, Ostwald growth at higher temperatures initiated phase transformation of the iron oxide nanoparticles and finished with the formation of the most stable phase—α-Fe_2O_3 phase. The presence of the porous, nonmagnetic matrix enables minimization of the nanoparticle interaction and enables the control of the particles size [53].

Synthesis factors of importance for every stage of the sol-gel synthesis are the choice/ratio of the precursors and pH. The influence of the variation of the synthesis conditions onto the properties of the final synthesis product is still not sufficiently investigated. What is known from the literature is that the influence of pH is reflected in the defining of the pore size. Base-catalyzed sol-gel synthesis conditioned slow hydrolysis of the alkoxide precursor and fast condensation. Final matrix pores are determined by the sizes from 2 to 50 nm [54]. In contrary, acid-catalyzed sol-gel synthesis favors rapid hydrolysis, consequently bringing to the formation of a huge number of small SiO_2 nuclei. The obtained gel consisted of the pores, with the size less than 2 nm [54]. This is explained by the influence of the hydrolysis and condensation rate on the formation of different polymers: base catalysis enabled formation of the longer, branched polymers, while acid catalysis resulted in the formation of linear polymers [55, 56]. Consequently, auto-, acid-, or base-catalyzed sol-gel syntheses could be used for the preparation of the α-Fe_2O_3/ SiO_2 nanocomposite, significantly different in its properties.

5. Coercivity of the composite nanomaterials

If someone needs to get a better insight in the biomedical application of nanocomposite materials based on hematite, it is important to understand in detail synthesis, reaction mechanism, and correlation between synthesis conditions and properties of prepared samples containing nano-hematite particles. Some basic magnetic properties of nano-hematite phase are not well-established up until today, which complicate its biomedical application. From a fundamental point of view, the understanding of coercivity behavior is of great importance because coercivity presents magnetic property that significantly influences and determines application of the investigated nanomaterial.

An obstacle in a determination of the precise coercivity value of nanocomposite materials consisting hematite nanoparticles presents often occurrence of the intermediate iron oxide phase—epsilon phase (ε-Fe₂O₃) that is obtained during the synthesis of high-temperature hematite phase, by sol-gel method. ε-Fe₂O₃ polymorph is formed in the course of Fe₃O₄/γ-Fe₂O₃ → α-Fe₂O₃ structural transformation and often coexisted concomitantly with the α-Fe₂O₃ phase. The situation is additionally complicated by the inability to clearly separate a temperature range during which pure hematite or epsilon phase is formed. Pure hematite phase could be synthesized by various synthesis approaches at different temperatures up to 1100°C, while the epsilon phase is obtained only by sol-gel method and still is not prepared pure.

Having in mind that the behavior of α-Fe₂O₃ and ε-Fe₂O₃ phases is still not properly understood, the primary question regarding H_{ci} value of nanocomposite materials containing hematite nanoparticles becomes: what is the difference between the mechanism of the coercivity field variations of the nano-hematite and nano-epsilon phase, since both of these phases could be characterized by coercivity field value ranging from zero to few thousand Oe?

To answer this question, more detailed scientific research should be performed. The correlation between H_{ci} value and material microstructure is not sufficiently understood neither for bulk nor for nanomaterials [57]. Intrinsic coercivity field presents a reverse field required to reduce the magnetization (M) from the remnant magnetization (M_r) again to zero. The main problem in interpretation of the intrinsic coercivity field value is that the field measured by magnetic devices is not the coercivity field, but some critical field influenced by the magnetic interactions [57]:

$$H_{crit} = H_{ci} + H_{int} \qquad (2)$$

When we deal with attempts to understand the origin of the coercivity field variations in nano-sized samples, of big importance is the independent analysis of the H_{crit} and H_{ci} values, which is difficult, since consensus about the factors that influence H_{int} and H_{ci} still is not achieved in the scientific community and presents a problem that should be overcome in the future.

The correlation between synthesis conditions and H_{ci} value occurred through the competition of different parameters, which influence and contribute in the different measure of the final H_{crit} and H_{ci} values. The mathematical expression that would describe dependence of H_{crit} on different parameters which influenced the coercivity field value has yet to be found, but roughly, it can be expressed as a function of different parameters (denoted according to the Greek alphabet) [Eq. (3)] [58]:

$$H_{crit} = f(\alpha, \beta, \gamma, \delta, \varepsilon, \eta, \theta, \iota, \kappa) \qquad (3)$$

The main influence on the coercivity value arises from:

a. Synthesis conditions (parameter α)

b. Presence of different iron oxide species in the investigated sample (parameter β)

c. Contribution originated from the physical and chemical properties of the SiO_2 matrix, such as pore size distribution or the flow of different gases through the matrix (parameter γ)

d. Angular distribution of the nanoparticle orientations (parameter δ)

e. Particle size and shape distribution (parameter ε)

f. An interplay between different inter- and intra-particle interactions in the nanoparticle system (parameter η)

g. Nanoparticle structural defects (denoted as parameter θ)

h. Anisotropy field (parameter ι)

i. Surface effects (κ)

In the next section, the impact of the parameters α and β on the measured magnetic field, that is in literature labeled as coercivity field, of the synthesized nanocomposite materials will be considered. X-ray diffraction and hysteretic measurements were performed in order to investigate the influence of the variation of synthesis parameters onto the formation of hematite phase as well as on the measured magnetic field value of the samples containing the pure hematite phase and hematite phase (as a dominant phase) in combination with the epsilon phase (appeared in traces). Few examples of the peculiar H_{crit} behavior of the investigated samples will be represented.

6. α-Fe_2O_3 nanoparticles prepared by auto-, acid-, and base-catalyzed sol-gel syntheses

In the following part, synthesis of the samples prepared by auto-, acid-, and base-catalyzed sol-gel methods will be described in detail. X-ray diffraction patterns and hysteretic measurements recorded at 200 K are shown. X-ray diffraction intensity is normalized. In the entire text, the value of the magnetization (M) is normalized so that $M_s = 1$. The normalized values of magnetization were introduced in order to avoid uncertainty in the estimation of the magnetization expressed in emu/g. Having in mind that H_{crit} presents magnetic field measured by magnetometer, H_{crit} will be labeled as H_{meas} in the figures of hysteresis.

6.1 Nano-hematite-based materials prepared by auto-catalyzed sol-gel synthesis

The auto-catalyzed sol-gel synthesis implied the dissolving of iron (III) nitrate nonahydrate ($Fe(NO_3)_3 \times 9H_2O$) in water in molar ratio 0.013:1 (catalyst solution),

while mixing of tetraethyl orthosilicate (TEOS), ethanol (C_2H_5OH), and water in molar proportion 1:12:12 enabled formation of alkoxide solution [59]. Solutions were mixed and stirred at room temperature. Gelation occurred during 36 days, afterward alcogel was dried for 5h at room temperature. Thermal treatment is performed in two ways. Alcogel is annealed in the air atmosphere for 3 h at 1050 and 1060°C as well as at 1050°C for 25 h. Investigated samples contained α-Fe_2O_3 as a dominant phase and smaller amount of the ε-Fe_2O_3 phase. Variation of the annealing conditions enables observation of the changes in the H_{crit} of the prepared samples, which is in detail discussed in Ref. [59].

6.1.1 Variation of the sol-gel synthesis conditions: alteration of the annealing conditions (temperature and time)

Diffraction pattern of the alcogel annealed at 1050°C for 3 h is presented in **Figure 1(a)** [59].

Hematite nanocrystallites (JCPDS card no.: 72-469) are observed as a dominant phase, while α-Fe_2O_3 phase (JCPDS card no.: 16-653) is presented in small amount. **Figure 2** presents hysteresis of the same sample [59]. Although the sample showed a higher amount of the α-Fe_2O_3 phase, measured critical field achieved a value characteristic for ε-Fe_2O_3 phase: 14.1 kOe (**Figure 2**) [59].

The increase of the annealing temperature for only 10°C (T_{ann} = 1060°C, t_{ann} = 3 h) resulted in the sharp decrease of H_{meas} (2300 Oe), which is shown in **Figure 2(a)** [59].

Observed behavior of measured critical field of the sample has been attributed to the completion of an ε-$Fe_2O_3 \rightarrow \alpha$-$Fe_2O_3$ phase transformation [59]; thus the presence of the only one phase—α-Fe_2O_3 phase—at 1060°C would be expected. With the aim to check the concluded remark regarding the completion of ε-$Fe_2O_3 \rightarrow \alpha$-$Fe_2O_3$ phase transformation at depicted temperature, investigation presented in Ref. [59] is continued by measuring the diffraction pattern of the sample annealed at 1060°C 3 h. Diffraction measurement (**Figure 2(b)**) revealed that, although the value of 2300 Oe could be characteristic for nano-sized α-Fe_2O_3 samples [24, 59], an investigated sample still contained the ε-Fe_2O_3 phase, although represented in the smaller amount than the sample annealed at 1050°C (**Figure 1(a)**).

On the other hand, published data reported more pronounced sharp decrease in H_{meas} value (600 Oe) for the sample performed to annealing at 1050°C for 25 h (**Figure 3(a)**). In order to confirm the completion of the ε-Fe_2O_3 to α-Fe_2O_3 phase transformation under these annealing conditions [59], investigation was continued by the measuring diffraction pattern of the mentioned sample (**Figure 3(b)**).
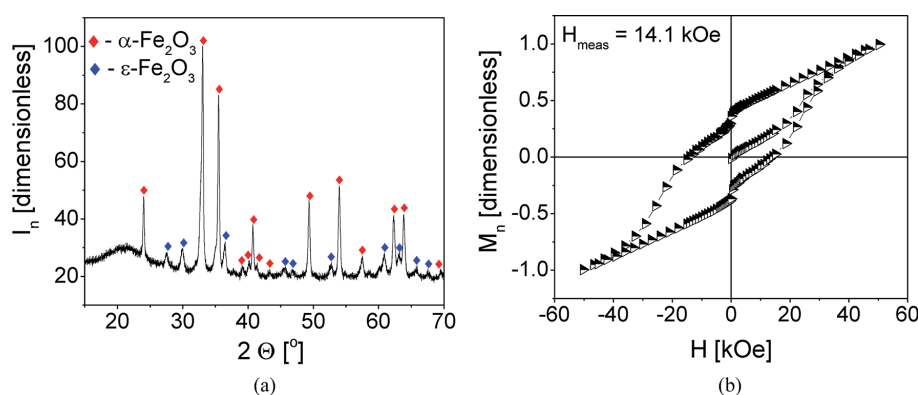
Figure 1.
Sample annealed at 1050°C for 3 h (a) diffraction pattern; (b) hysteretic curves [59].
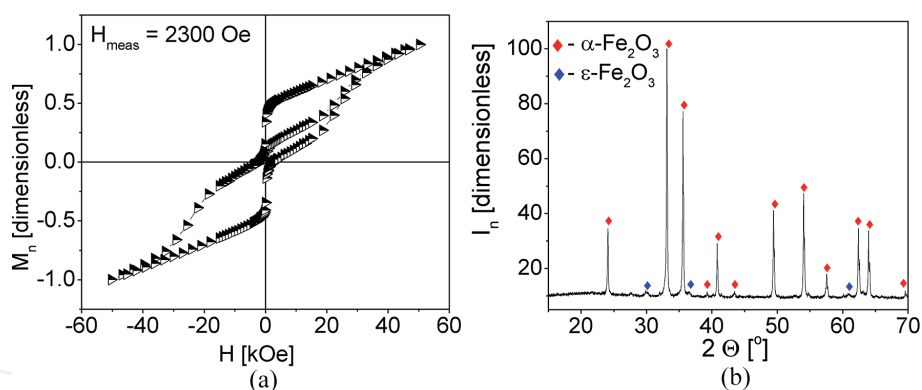
Figure 2.
Sample annealed at 1060°C for 3 h: (a) hysteretic curves [59]; (b) diffraction pattern.
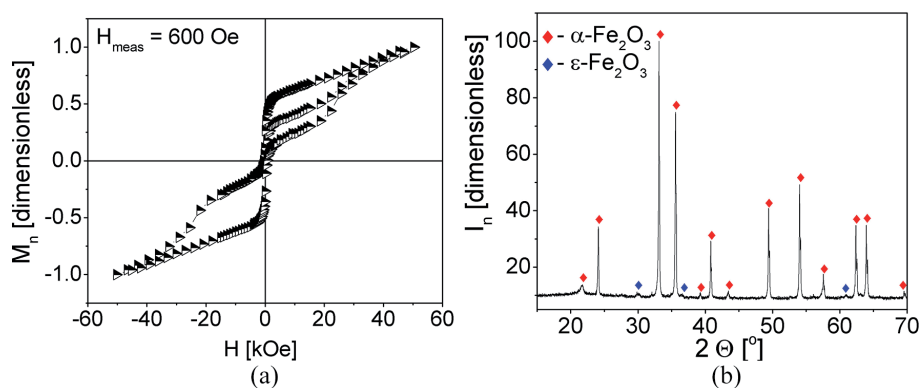
Figure 3.
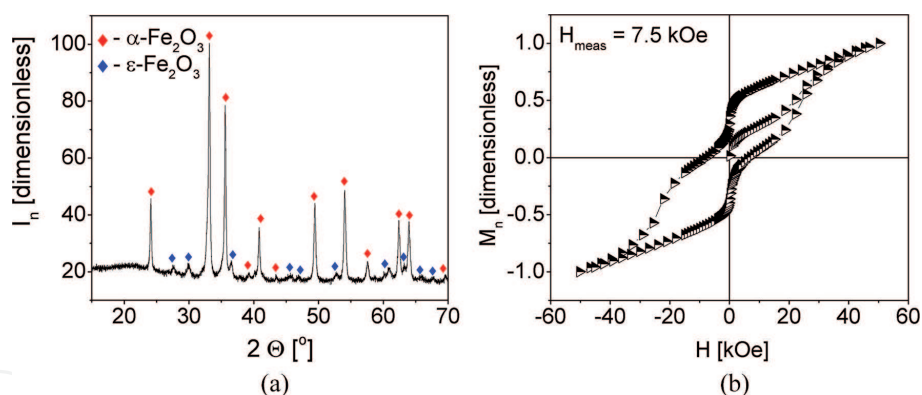*Sample annealed at 1050°C for 25 h: (a) hysteretic curves [59]; (b) diffraction pattern.*

In spite of a very long annealing treatment (25 h), the traces of the epsilon phase is still presented ($2\theta = 30.25°$) at the diffraction pattern presented in **Figure 3(b)**, although H_{meas} was very low for the epsilon phase, 600 Oe (**Figure 3(a)**).

Observed results pointed to the often mistakes in the scientific literature, where is sharp decrease in the measured magnetic field (H_{meas}) of the samples containing hematite and epsilon phases attributed to the finish of the $\varepsilon\text{-}Fe_2O_3 \rightarrow \alpha\text{-}Fe_2O_3$ phase transformation. In other words, vanishing of the huge value of the measured field (which is in the articles denoted as Hc) of the probed samples is obviously not a conclusive evidence that is pointing to the absence of epsilon phase in the sample and which could confirms completion of the $\varepsilon\text{-}Fe_2O_3 \rightarrow \alpha\text{-}Fe_2O_3$ transformation.

6.1.2 Variation of the sol-gel synthesis conditions: alteration of the iron precursor initial amount

Further research of the variation of the sol-gel synthesis parameters directed the investigation in the course of altering of the amount of the iron precursor, $Fe(NO_3)_3\cdot9H_2O$. The sample is synthesized by the identical auto-catalyzed sol-gel procedure used for the preparation of the former discussed samples, with the only difference that the molar ratio of $Fe(NO_3)_3\cdot9H_2O$ and water was 0.017:1 [60]. Alcogel is annealed at 1030°C for 3 h in the air atmosphere. Diffraction pattern is shown in **Figure 4(a)** [60].

Figure 4(a) revealed that $\alpha\text{-}Fe_2O_3$ phase is recognized as a dominant phase, and $\varepsilon\text{-}Fe_2O_3$ phase as an impurity. Noteworthy, comparison of **Figures 4(a)** and **1(a)** pointed to pronounced similarities between phase compositions of the investigated samples. Surprisingly, hysteretic measurements revealed that, in spite of nearly the

Figure 4.
Sample annealed at 1050°C for 3 h (reduced content of the iron precursor): (a) diffraction pattern;
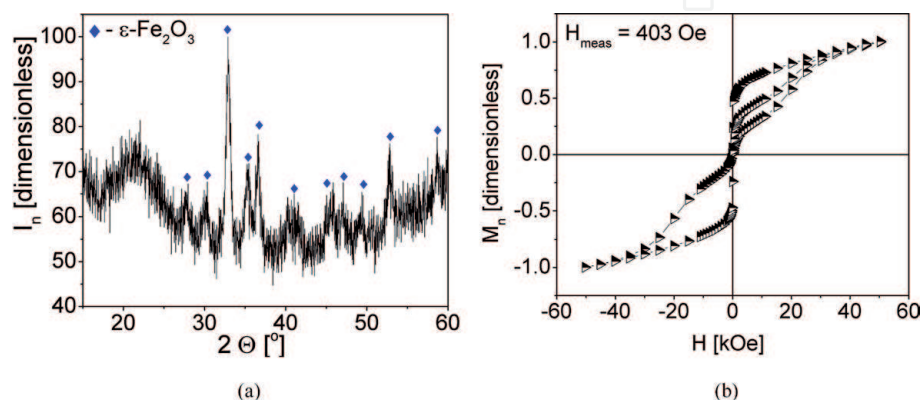*(b) hysteretic curves [59].*

same diffraction patterns, the examined sample showed significantly lower value of measured magnetic field, 7.5 kOe [60]. Deeper analysis, that is out of the objective of this chapter but in detail explained elsewhere [60], showed that the origin of the H_{meas} value variations occurred as a consequence of the increased amount of the SPM nanoparticles within the investigated sample [60].

6.1.3 Variation of the sol-gel synthesis conditions: alteration of the iron (III) nitrate precursor

Hydrated iron (III) nitrate shows high non-stability and tendency to absorb humidity from the air [61]. To ensure avoidance of the contact with the air, the best way is to prepare iron (III) nitrate directly from the elemental iron and nitric acid solution. In order to investigate behavior of measured magnetic field of the sample prepared by auto-catalyzed sol-gel synthesis with the usage of anhydrous iron nitrate (instead of nonahydrated iron (III) nitrate) as a precursor, the next procedure is performed: catalyst solution is prepared by the dissolving of iron (III) nitrate in water in molar ratio 0.007:1. Alkoxide solution is prepared by mixing tetraethyl orthosilicate (TEOS), ethanol (C_2H_5OH), and water in molar proportion 1:6:6. Mixed solutions are stirred for 5 h. Gelation takes place in 20 days. Gel is dried for 19 h at 80°C and afterward is annealed at 1030°C for 3 h.

Diffraction pattern of the sample is shown in **Figure 5(a)**.

Figure 5(a) depicted the complete absence of the α-Fe₂O₃ phase and presence of the ε-Fe₂O₃ phase as the only observed iron oxide phase in the sample. Hysteretic

Figure 5.
Sample annealed at 1030°C for 3 h (anhydrous Fe(NO₃)₃ used as a precursor): (a) diffraction pattern;
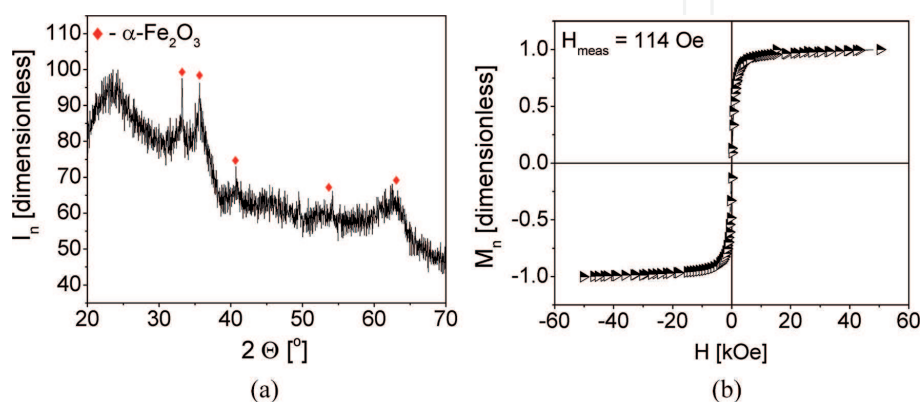*(b) hysteretic curves.*

measurement of this sample is shown in **Figure 5(b)**. Interestingly, magnitude of the measured magnetic field of the sample was ~400 Oe. Since literature data showed that this Fe_2O_3 polymorph is characterized by high H_{ci} (10–20 kOe) [29–31] or by SPM behavior (H_{ci} ~ 0 Oe) [33], mentioned Hmeas value is not characteristic neither for high coercivity ε-Fe_2O_3 nor for the SPM ε-Fe_2O_3 phase. Moreover, obtained value is similar to the case presented in **Figure 3(b)**, where it is observed that the sample, containing the α-Fe_2O_3 as a dominant phase, showed H_{meas} ~ 600 Oe. It is important to notice here that an alcogel of the sample whose diffraction pattern is represented in the **Figure 1(a)**, performed to the thermal treatment under the similar annealing conditions, is characterized by the value of the measured magnetic field of 14.1 kOe, although hematite phase was presented as a dominant [59]. Further research of this sample will be performed by Mossbauer spectroscopy, in order to discuss the observed measured magnetic field behavior of the sample in detail.

6.2 Nano-hematite-based materials prepared by acid-catalyzed sol-gel synthesis

In order to investigate the influence of the catalyst in the sol-gel synthesis of hematite nanoparticles, a sample is synthesized by acid sol-gel synthesis route [62]. This synthesis method is similar to auto-catalyzed synthesis procedure, with the difference that nitric acid (HNO_3) is used as a catalyst. Tetraethyl orthosilicate, ethanol, iron (III) nitrate nonahydrate, and nitric acid were mixed in a molar ratio of 1:3:0.2:10. Solution is magnetically stirred for 1 h at room temperature. Gelation took place for 20 days. Obtained gel is dried at 80°C for 19 h, after which it is subjected to thermal treatment under the air atmosphere at temperature of 800°C for 2 h.

Figure 6(a) presents a diffraction pattern of the investigated sample. Pure α-Fe_2O_3 phase is observed as the only iron oxide phase. Hematite nanoparticles are observed at lower temperature than investigated examples characterized by diffraction patterns shown in **Figures 1(a)** and **4(a)**.

Corresponding hysteretic curves are shown in **Figure 6(b)**, pointing to the presence of hematite phase as the only iron oxide phase. Measured magnetic field of the α-Fe_2O_3/SiO_2 sample achieved the value of 114 Oe, which is ascribed to the coercivity of hematite nanoparticles. Accordingly, the presence of the catalyst enabling the accelerated formation of the hematite phase at lower temperatures (samples examined in **Figures 1–4** revealed the appearance of hematite phase at temperatures higher than the sample presented at **Figure 6** [59, 60]).

Figure 6.
Sample annealed at 800°C for 2 h (HNO_3 used as a catalyst): (a) diffraction pattern [62]; (b) hysteretic curves.

### 6.3 Nano-hematite-based materials prepared by base-catalyzed sol-gel synthesis

Literature review confirmed that acid-catalyzed sol-gel synthesis enabled the preparation of the samples characterized by various phase transformation routes resulting in the formation of *α-Fe$_2$O$_3$* phase: spinel phase (Fe$_3$O$_4$/γ-Fe$_2$O$_3$) → rhombohedral phase (α-Fe$_2$O$_3$) as well as spinel (Fe$_3$O$_4$/γ-Fe$_2$O$_3$) → orthorhombic (ε-Fe$_2$O$_3$) → rhombohedral (α-Fe$_2$O$_3$) phase. Dependent on the synthesis conditions, different H$_{meas}$ values of the samples are recorded [27]. On the other hand, base-catalyzed synthesis in combination with inverse micelle method is characterized by the phase transformation route Fe$_3$O$_4$/γ-Fe$_2$O$_3$ → ε-Fe$_2$O$_3$ → α-Fe$_2$O$_3$ and presents a highly reproducible method for synthesis of high-temperature nano-hematite particles. The influence of the post-annealing treatment onto the H$_{meas}$ value of the samples prepared by this type of sol-gel method is investigated in Ref. [63].

In the method described below, nano-hematite particles are obtained after post-annealing treatment of the samples prepared in base-catalyzed sol-gel synthesis in combination with the microemulsion method [64, 65]. Two identical microemulsions, containing water, cetyltrimethyl ammonium bromide (CTAB), buthanol, and n-octan, were mixed in a particular moral ratio. CTAB is an agent which facilitates formation of the matrix pores in the desired size [54]. Octan presents the solvent that enables the mixing of the reactants, while usage of alcohol of the somewhat longer chain (butanol) ensures a shortened time of the condensation reactions. In one microemulsion Sr^{2+} is added, whose role is the acceleration of the particle growth along one crystallographic axis, resulting in the rod morphology of the nanoparticles [64]. In another microemulsion a base catalyst, ammonia, is added that possesses a significant role in the defining of the SiO$_2$ pore size. Mixing the microemulsions enables stirring of the solution. Afterwards, TEOS is added in the precise stechiometrical ratio. Gao et al. [66] confirmed that the ideal volume ratio of the TEOS and alcohol (desirable in order to shorten the gelation time) is 1:2, while the same effect is achieved by simultaneously mixing the TEOS and NH$_3$ in the volume ratio 2:5.

6.3.1 Variation of the sol-gel synthesis conditions: post-annealing treatment

Having in mind that the influence of the annealing conditions on the samples synthesized by this method is well-established in literature [64, 65], obtained samples were performed to post-annealing treatment in order to investigate coercivity behavior of the samples post-annealed at low temperature (100°C) and high temperature (1100°C) [63, 67].

The synthesis of the sample comprised the preparation of two identical micelles, consisting of CTAB, isooctane, butanol, and water in the molar ratio—0.03:0.33:0.12:1.00. Iron (III) nitrate (prepared by dissolving elemental iron in nitric acid and water) is added to the water in the molar ratio 0.00047:1. In the first micelles precursors of the iron and strontium ions in molar ratio 3:1 are added. In another micelle 0.09 mol of ammonia is added. After mixing the micelles, TEOS is dropped into the stirred solution (volume ratio of TEOS and ammonia was 4.5:1.7, while volume ratio of the TEOS and butanol was 4.5:10.7). Solution is stirred for 24 h. Afterward, precipitate is collected and treated with a chloroform and ethanol in order to wash organic moistures, attached to the surface of the precipitated nanoparticles. A coprecipitate has been annealed at 1050°C for 4 h. The same amounts of the sample are performed to the post-annealing treatment [63].
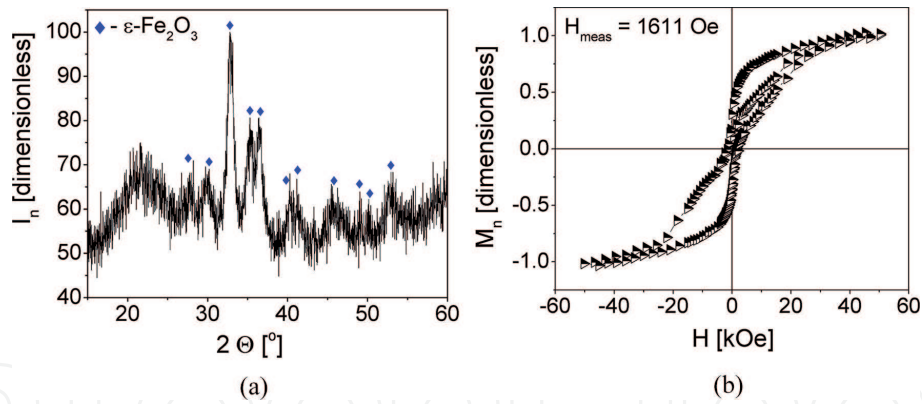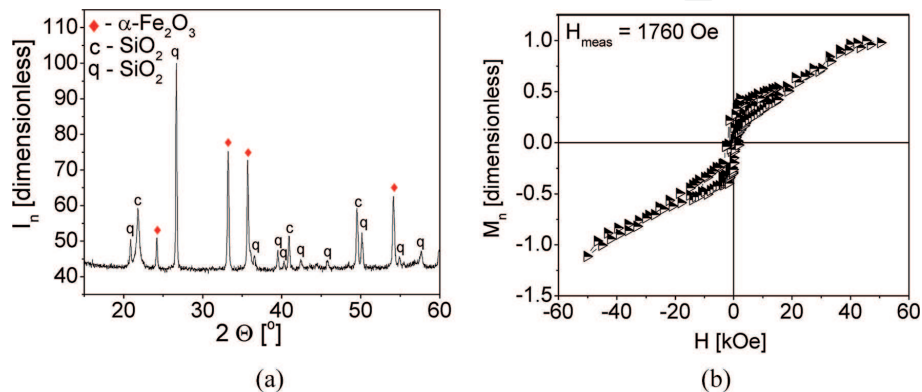
Figure 7.
Sample annealed at 1050°C for 4 h, post-annealed at 100°C for 3 h: (a) diffraction pattern; (b) hysteretic curves [60].

Diffraction pattern of the sample post-annealed at 100°C is shown in **Figure 7(a)** [67]:

The only noticed phase was the ε-Fe_2O_3 phase. In order to examine its magnetic behavior, hysteretic curves are measured and shown in the **Figure 7(b)** [67]. Measured magnetic field of the sample was 1611 Oe. Literature data showed that obtained value is not exactly characteristic for epsilon phase coercivity, and it would be more appropriate to ascribe that H_{meas} value to hematite phase, then for epsilon. According to **Figure 7(b)** and the literature data [67], it can be concluded that post-annealing treatment at 100°C brings to the drastic drop of measured measured magnetic field value. Before post-annealing treatment, sample annealed at 1050°C for 4 h showed measured magnetic field value of 21.3 kOe [63], although the phase composition of the sample was the same [67]. This fact underlined that sharp changes in the H_{meas} value of the nanocomposite samples prepared by sol-gel method could not be ascribed to Fe_2O_3 polymorph transformations.

To get a better insight in the H_{meas} variations initiated by post-annealing treatment, the piece of alcogel annealed at 1050°C for 4 h was performed to the post-annealing treatment at 1100°C for 3 h [63].

Figure 8(a) revealed that the only observed iron oxide phase is pure α-Fe_2O_3 phase [63], pointing to the ending of the ε-Fe_2O_3 to α-Fe_2O_3 phase transformation. In diffraction pattern is in addition noticed change of the silica matrix, converted from amorphous silica to highly crystalline cristoballite (JCPDS card no.: 39-1425) and quartz phase (JCPDS card no.: 46-1045) [56, 63]. Interestingly, hysteretic curves shown in **Figure 8(b)** exerted measured magnetic field value of 1760 Oe

Figure 8.
Sample annealed at 1050°C for 4 h, post-annealed at 1100°C for 3 h: (a) diffraction pattern (letter "c" referred to cristoballite SiO_2 phase; letter "q" referred to quartz SiO_2 phase); (b) hysteretic curves [49].

that is quite similar to the measured value of the sample post-annealed at 100°C ($H_{meas} \sim$ 1600 Oe). Noteworthy, **Figures 7(b)** and **8(b)** showed a similar values of measured magnetic field of the samples consisted of obviously different phases (**Figures 7(a)** and **8(a)**), pointing to the potential usage of the samples consisted of α-Fe₂O₃ and ε-Fe₂O₃ together (as in the case of "SPION" species), although this claim requires deeper investigation of magnetic properties of the samples.

Conclusively, it is important to notice that all hysteretic curves (except **Figure 6(b)**), referring to the sample containing the only hematite phase, observed at lower temperature in comparison with the other investigated samples) could be classified as hysteretic loops having constricted middles (wasp-waisted loops). Generation of wasp-waisting curves appears as a result of two population of the particles characterized by distinct coercivity spectra; numerical simulations reveals that wasp-waisting curves requires and SPM contribution [68], that is confirmed by **Figures 4(b)** and **1(b)** [58]. Experimental results shown in **Figures 2(a)** and **3(a)** revealed that the decrease of measured magnetic field value of the samples is not a certain parameter that indicates vanishing of the other iron oxide polymorphs and the presence of the pure hematite nanoparticles. Moreover, represented results pointed out that ε-Fe₂O₃ → α-Fe₂O₃ phase transformation cannot be the decisive factor on the coercivity value of the nanocomposite material (**Figures 1**–**4**) [58]. The variation of the initial iron ion precursor amount [60] enables the alteration of measured magnetic field value without changing the phase composition of the nanocomposite material. The usage of anhydrous Fe^{3+} precursor and change of the precursor ratio during synthesis cause the significant alterations of the phase composition of the investigated samples and differences in H_{meas} value (**Figures 1** and **5**). Appearance of the catalyst accelerated phase transformations of the Fe₂O₃ polymorph and favors the obtaining of the pure nano-hematite phase (**Figure 6(a)**).

Noteworthy, nanocomposite samples containing different phase compositions could be characterized by a significantly similar measured magnetic field values. This is confirmed by examination of the samples prepared by auto-catalyzed sol-gel synthesis (**Figures 3** and **5**) and samples synthesized by base-catalyzed sol-gel method (**Figures 7** and **8**). An observed feature is pointing to the fact that coercivity of the nanocomposite materials could not be mainly driven by the parameters α and β from Eq. (2). The results represented in this chapter indicated the necessity of taking other parameters [parameters: $\gamma - \kappa$, Eq. (2)] into consideration, in order to understand properly the coercivity behavior of nanocomposite materials.

6.4 TEM measurements

An important issue in the characterization of the nanoparticles presents transmission electron microscopy (TEM). In order to understand the distribution of

(a)   (b)
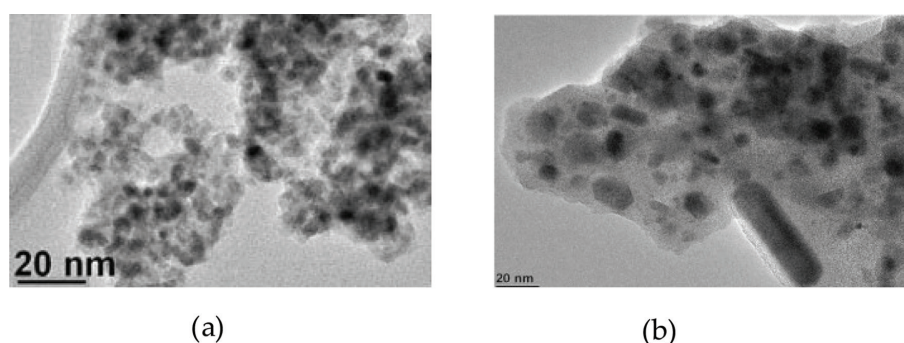
Figure 9.
TEM micrographs of the sample: (a) prepared by auto-catalyzed sol-gel synthesis, annealed at 1050°C for 3 h [52], left; (b) prepared by base-catalyzed sol-gel synthesis, annealed at 1050°C for 4 h [56], right.

nano-hematite particles, TEM micrographs of the chosen nanocomposite samples annealed at 1050°C, obtained by auto-catalyzed and base-catalyzed sol-gel synthesis routes, are shown in **Figure 9(a)** and **(b)**.

Detailed TEM analysis is given in Ref. [59, 63]. Quantitative description of morphological properties of the investigated particles is performed by measuring ellipticity. The results of the analysis showed that the shape of observed Fe_2O_3 nanoparticles (ε-Fe_2O_3 and α-Fe_2O_3) varies from ellipticity to circularity. In other words, **Figure 9** confirms the presence of nonideally spherical particles, whose shape deviates from circularity in a different measure [59]. Fe_2O_3 particle sizes, presented in **Figure 9(a)**, are ranging between 10 and 20 nm, while the sample presented in **Figure 9(b)** showed a wider particle size distribution, from 4 to 50 nm, and the same variations from ellipticity to circularity. Wide size distribution leads to the presence of different particle shapes during the annealing treatment, elliptic/spherical (**Figure 9(a)**). This feature appeared as a consequence of the fact that sol-gel method consisted of coprecipitation of the particles within the SiO_2 pores (coprecipitated samples are characterized by wide particle size distribution) [53]. The best way to overcome the mentioned problem is the coating of the nanoparticles within the SiO_2 pores [69].

Notwithstanding, a significant difference between micrographs is the presence of nanorod particles within the sample synthesized by base-catalyzed sol-gel synthesis (**Figure 9(b)**). Rod-like morphology appeared as a consequence of the participation of group II element, Sr^{2+}, in the synthesis procedure (**Figure 9(b)**). The addition of Sr^{2+} ions accelerated the growth of the ε-Fe_2O_3 particles in one crystallographic axis [63], inducing more pronounced shape variations and formation of rod-like nanoparticles. If we recall the fact that TEM image shown in **Figure 9(b)** revealed the presence of the only γ-Fe_2O_3 and ε-Fe_2O_3 nanoparticles in the investigated sample (discussed in more detail in the Ref. [63]), as well as having in mind that α-Fe_2O_3 formation occurs as a consequence of phase transformations ε-$Fe_2O_3 \rightarrow \alpha$-$Fe_2O_3$, it can be assumed that the sample presented in **Figure 8** contained rod-like α-Fe_2O_3 nanoparticles.

It is important to note that the origin of dependence of H_{meas} behavior on the synthesis conditions of the samples investigated in this chapter is found in quantum mechanics.

Briefly, the quantity that strongly affects the shape of hysteresis loop is magnetic anisotropy [parameter ι, in Eq. (3)]. For the most simplest case, in crystal systems whose symmetry is determined by a single axis of high symmetry (uniaxial symmetry), anisotropy energy is defined as:

$$E_a \sim KV\sin^2\theta \tag{4}$$

where K is the anisotropy constant, V is the volume, and θ is the angle between two spins with respect to each other [17]. The overall magnetic anisotropy energy is dependent on the symmetry of the investigated systems and defined by various contributions, such as magnetocrystalline anisotropy, shape anisotropy, surface anisotropy, strain anisotropy and stress anisotropy.

Anisotropy energy appeared as a consequence of spin-orbit interaction and the partial quenching of the angular momentum [17]. From the aspect of nanomaterial preparation and dependence of samples of magnetic properties on synthesis conditions (annealing temperature and time), it is important to emphasize that the anisotropy constant is strongly temperature dependent [17]. Independent of the presence of the same or different iron oxide polymorph phases within the sample, differences in the structure and morphology characteristics of each individual nanoparticle resulted in the changes in a magnetic anisotropy.

Noteworthy, alteration of the SiO_2 matrix during the annealing treatment impacts magnetic properties of the samples [59]. Gas diffusion in the SiO_2 matrix,

initiated by thermal treatment, caused the crystallization of the amorphous matrix and changes in the size of the pores. Coalescing of the pores resulted in the alterations of the distance between magnetic nanoparticles within the pores [59], consequently influencing the magnetic behavior of the samples.

7. Conclusion

The main message of this chapter was to emphasize the importance of the investigation of the influence of the synthesis parameter variations onto the magnetic properties of the composite materials containing nano-hematite particles that could be used as a starting material for preparation of multifunctional nanoparticles, used in different areas of biomedicine. Since coercivity field presents a parameter of importance for application of this type of materials, alterations of measured measured H_{crit} value, initiated by changing the synthesis parameters, are discussed. To get a better insight into relation between synthesis conditions and magnetic properties of composites containing α-Fe$_2$O$_3$ nanoparticles, sol-gel synthesis is recognized as a suitable preparation method. Alterations of measured H_{crit} value of the samples are driven by the variation of the pH of the performed sol-gel synthesis (auto-, acid-, or base-catalyzed), initial Fe^{3+} and Si^{4+} precursor ratio, amount of the iron precursor, and annealing conditions (T and t) and by performing post-annealing treatment. The author expected that this chapter will facilitate a current and objective evaluation of the knowledge regarding the search for the exact mathematical expression of the measured intrinsic coercivity field value of the composite nanomaterials containing nano-hematite phase, which is of significance for improvement of the preparation of a high-quality nano-α-Fe$_2$O$_3$ particles for biomedical application.

Acknowledgements

Author details

Violeta N. Nikolić
Laboratory for Theoretical Physics and Condensed Matter Physics, Institute of Nuclear Sciences Vinča, University of Belgrade, Serbia

*Address all correspondence to: violeta@vinca.rs

IntechOpen

References

[1] Cornell RM, Schwertmann U. The Iron Oxides: Structure, Properties, Reactions, Occurrence and Uses. Weinheim, Germany: VCH; 2003

[2] Glasby GP, Schulz HD. Eh-Ph diagrams for Mn, Fe, Co, Ni, Cu and as under seawater conditions: Application of two new types of eh ph diagrams to the study of specific problems in marine geochemistry. Aquatic Geochemistry. 1999;**5**(2):227-248

[3] Ling Y, Wheeler DA, Zhang JZ, Li Y. Optical properties and applications of hematite (α-Fe_2O^3) nanostructures. In: One-Dimensional Nanostructures: Principles and Applications. New York: John Wiley & Sons, Inc; 2012. pp. 167-184

[4] Kefeni KK, Msagati TA, Nkambule TT, Mamba BB. Synthesis and application of hematite nanoparticles for acid mine drainage treatment. Journal of Environmental Chemical Engineering. 2018;**6**(2):1865-1874

[5] Shinde SS, Bansode RA, Bhosale CH, Rajpure KY. Physical properties of hematite α-Fe_2O_3 thin films: Application to photoelectrochemical solar cells. Journal of Semiconductors. 2011;**32**(1):013001-013003

[6] Morel D. Hematite: Sources, Properties and Applications. New York: Nova Science Publishers Incorporated; 2013

[7] Ling Y, Li Y. Review of Sn-doped hematite nanostructures for photoelectrochemical water splitting. Particle & Particle Systems Characterization. 2014;**31**(11):1113-1121

[8] Rao BN, Padmaraj O, Kumar PR, Venkateswarlu M, Rao VM, Satyanarayana N. Synthesis of hematite α-Fe_2O_3 nanospheres for lithium ion battery applications. AIP Conference Proceedings. 2015;**1665**(1):060014

[9] Kurata T, Katamoto T, Hiriishi N, Kiyama M. U.S. Patent No. 5,133,805. Washington, DC: U.S. Patent and Trademark Office; 1992

[10] Oliveira HS, Almeida LD, de Freitas VA, Moura FC, Souza PP, P P, et al. Nb-doped hematite: Highly active catalyst for the oxidation of organic dyes in water. Catalysis Today. 2015;**240**(1):176-181

[11] Pokropivny VV, Skorokhod VV. Classification of nanostructures by dimensionality and concept of surface forms engineering in nanomaterial science. Materials Science and Engineering: C. 2007;**27**(5-8):990-993

[12] Bodker F, Hansen MF, Koch CB, Lefmann K, Morup S. Magnetic properties of hematite nanoparticles. Physical Review B. 2000;**61**(10):6826-6829

[13] Catti M, Valerio G, Dovesi R. Theoretical study of electronic, magnetic and structural properties of α-Fe_2O_3 (hematite). Physical Review B. 1995;**51**(12):6789-6921

[14] Zhu M, Wang Y, Meng D, Qin X, Diao G. Hydrothermal synthesis of hematite nanoparticles and their electrochemical properties. Journal of Physical Chemistry C. 2012;**116**(30):16276-16285

[15] Li X, Zhao T, Sun L, Aifantis K, Fan Y, Feng Q, et al. The applications of conductive nanomaterials in the biomedical field. Journal of Biomedical Materials Research Part A. 2016;**104**(1):322-339

[16] Oles A, Kajzar F, Jucab M, Sikora W. Magnetic Structures

Determined by Neutron Diffraction. Warszava-Krakov: Panstwore Wydawnicto Naukome; 1976

[17] Blundell S. Magnetism in Condensed Matter. New York: Oxford University Press, Inc; 2003

[18] Kittel C. Introduction to Solid State Physics. New York: John Willey & Sons; 1996

[19] Klabunde NA. Nanoscale Materials in Chemistry. New York: John Willey & Sons; 2010

[20] Xu S, Habib AH, Gee SH, Hong YK, McHenry ME. Spin orientation, structure, morphology, and magnetic properties of hematite nanoparticles. Journal of Applied Physics. 2015;**117**(17):17A315. DOI: 10.1063/1.4914059

[21] Klein S, Sommer A, Distel LV, Neuhuber W, Kryschi C. Superparamagnetic iron oxide nanoparticles as radiosensitizer via enhanced reactive oxygen species formation. Biochemical and Biophysical Research Communications. 2012;**425**(2):393-397

[22] Barhoumi L, Dewez D. Toxicity of superparamagnetic iron oxide nanoparticles on green alga Chlorella vulgaris. BioMed Research International. 2013;**2013**:1-11. DOI: 10.1155/2013/647974

[23] Hill AH, Jiao F, Bruce PG, Harrison A, Kockelmann W, Ritter C. Neutron diffraction study of mesoporous and bulk hematite α-Fe₂O₃. Chemistry of Materials. 2008;**20**(1):4891-4899

[24] Tadic M, Citakovic N, Panjan M, Stanojevic B, Markovic D, Jovanovic D, et al. Synthesis, morphology and microstructure of pomegranate-like hematite (α-Fe₂O₃)

superstructure with high coercivity. Journal of Alloys and Compounds. 2012;**543**(5):118-124

[25] King JW, Channel ET. Sedimentary magnetism, environmental magnetism, and magnetostratigraphy. International Union of Geodesy and Geophysics. 1987;**29**(1):358-360

[26] Kurmoo M, Rehspringer JL, Hutlova A, Dorleans C, Vilminot S, Estournes C, et al. Formation of nanoparticles of ε-Fe₂O₃ from yttrium iron garnet in a silica matrix: Unusually hard magnet with a Morin-like transition below 150 K. Chemistry of Materials. 2005;**17**(1):1106-1114

[27] Popovici M, Gich M, Niznansky D, Roig A, Savii C, Casas L, et al. Optimized synthesis of the elusive ε-Fe₂O₃ phase via sol-gel chemistry. Chemistry of Materials. 2004;**25**(1):5542-5548

[28] Gich M, Gazquez J, Roig A, Crespi A, Fontcuberta J, Idrobo JC, et al. Epitaxial stabilization of ε-Fe₂O₃(00l) thin films on SrTiO₃(111). Applied Physics Letters. 2010;**96**(1):112508-112511

[29] Barick KC, Varaprasad BCS, Bahadur D. Structural and magnetic properties of γ- and ε-Fe₂O₃ nanoparticles dispersed in silica matrix. Journal of Non-Crystalline Solids. 2010;**356**(1):153-159

[30] Yakushkin SS, Balaev DA, Dubrovskiy AA, Semenov SV, Shaikhutdinov KA, Kazakova MA, et al. Evolution of the Fe³⁺ ion local environment during the phase transition ε-Fe₂O₃→α-Fe₂O₃. Journal of Superconductivity and Novel Magnetism. 2018;**31**(4):1209-1217

[31] Liu J, Qiao SZ, Chen JS, Lou XWD, Xing X, Lu GQM. Yolk/ shell nanoparticles: New platforms for

nanoreactors, drug delivery and lithium-ion batteries. Chemical Communications. 2011;**47**(47):12578-12591

[32] Lu C, Liu X, Li Y, Yu F, Tang L, Hu Y, et al. Multifunctional janus hematite-silica nanoparticles: Mimicking peroxidase-like activity and sensitive colorimetric detection of glucose. ACS Applied Materials & Interfaces. 2015;**7**(28):15395-15402

[33] Yu BY, Kwak SY. Carbon quantum dots embedded with mesoporous hematite nanospheres as efficient visible light-active photocatalysts. Journal of Materials Chemistry. 2012;**22**(17):8345-8353

[34] Yin ZF, Wu L, Yang HG, Su YH. Recent progress in biomedical applications of titanium dioxide. Physical Chemistry Chemical Physics. 2013;**15**(14):4844-4858

[35] Mirzaei A, Janghorban K, Hashemi B, Bonyani M, Leonardi SG, Neri G. Highly stable and selective ethanol sensor based on α-Fe$_2$O$_3$ nanoparticles prepared by Pechini sol–gel method. Ceramics International. 2016;**42**(5):6136-6144

[36] Selvam AP, Muthukumar S, Kamakoti V, Prasad S. A wearable biochemical sensor for monitoring alcohol consumption lifestyle through ethyl glucuronide (EtG) detection in human sweat. Scientific Reports. 2016;**6**(2):23111-23114

[37] Kim DH, Shim YS, Jeon JM, Jeong HY, Park SS, Kim YW, et al. Vertically ordered hematite nanotube array as an ultrasensitive and rapid response acetone sensor. ACS Applied Materials & Interfaces. 2014;**6**(17):14779-14784

[38] Rohr TE. U.S. Patent No. 5,445,971. Washington, DC: U.S. Patent and Trademark Office; 1995

[39] Litvinov D, Willson R. U.S. Patent No. 8,456,157. Washington, DC: U.S. Patent and Trademark Office; 2013

[40] Bhar R, Kaur G, Mehta SK. Exploring drying pattern of a sessile droplet of genomic DNA in the presence of hematite nanoparticles. Scientific Reports. 2018;**8**(1):6352-6355

[41] Lu Y, Yin Y, Mayers BT, Xia Y. Modifying the surface properties of superparamagnetic iron oxide nanoparticles through a sol–gel approach. Nano Letters. 2002;**2**(3):183-186

[42] Cui H, Liu Y, Ren W. Structure switch between α-Fe$_2$O$_3$, γ-Fe$_2$O$_3$ and Fe$_3$O$_4$ during the large scale and low temperature sol–gel synthesis of nearly monodispersed iron oxide nanoparticles. Advanced Powder Technology. 2013;**24**(1):93-97

[43] Gupta AK, Gupta M. Synthesis and surface engineering of iron oxide nanoparticles for biomedical applications. Biomaterials. 2005;**26**(18):3995-4021

[44] Li Z, Barnes JC, Bosoy A, Stoddart JF, Zink JI. Mesoporous silica nanoparticles in biomedical applications. Chemical Society Reviews. 2012;**41**(7):2590-2605

[45] Tartaj P, del Puerto Morales M, Veintemillas-Verdaguer S, Gonzalez-Carreno T, Serna CJ. The preparation of magnetic nanoparticles for applications in biomedicine. Journal of Physics D: Applied Physics. 2003;**36**(13):R182-R197

[46] Salata OV. Applications of nanoparticles in biology and medicine. Journal of Nanobiotechnology. 2004;**2**(1):3-6

[47] Jesus M, Penades S. Glyconanoparticles: Types, synthesis and applications in glycoscience, biomedicine and material science.

Biochimica et Biophysica Acta (BBA)-General Subjects. 2006;**1760**(4):636-651

[48] Neuberger T, Schopf B, Hofmann H, Hofmann M, Von Rechenberg B. Superparamagnetic nanoparticles for biomedical applications: Possibilities and limitations of a new drug delivery system. Journal of Magnetism and Magnetic Materials. 2005;**293**(1):483-496

[49] Nitin N, LaConte LEW, Zurkiya O, Hu X, Bao G. Functionalization and peptide-based delivery of magnetic nanoparticles as an intracellular MRI contrast agent. Journal of Biological Inorganic Chemistry. 2004;**9**(6):706-712

[50] Lopez-Sanchez J, Serrano A, Del Campo A, Abuin M, Rodriguez de la Fuente O, Carmona N. Sol–gel synthesis and micro-raman characterization of ε-Fe₂O₃ micro-and nanoparticles. Chemistry of Materials. 2016;**28**(2):511-518

[51] Taboada E, Gich M, Roig A. Nanospheres of silica with an ε-Fe₂O₃ single crystal nucleus. ACS Nano. 2009;**3**(11):3377-3382

[52] Akbar S, Hasanain SK, Azmat N, Nadeem M. Synthesis of Fe₂O₃ nanoparticles by new sol-gel method and their structural and magnetic characterizations. arXiv preprint cd-mat/04084802004. pp. 1-9

[53] Zhang J, Chen X, Shen Y, Li Y, Hu Z, Chu J. Synthesis, surface morphology, and photoluminescence properties of anatase iron-doped titanium dioxide nano-crystalline films. Physical Chemistry Chemical Physics. 2011;**13**(28):13096-13105

[54] Stober W, Fink A, Bohn E. Controlled growth of monodisperse silica spheres in the micron size range. Journal of Colloid and Interface Science. 1968;**26**(1):62-69

[55] Brinker CJ, Scherer GW. Sol-Gel Science, The Physics and Chemistry of Sol-Gel Processing. New York: Academic Press; 1990

[56] Nikolic VN. Магнетне особине наночестица оксида гвожђа површински модификованих силицијум диоксидом и олеинском киселином [PhD dissertation]. Serbia: INN "Vinca", University of Belgrade; 2017

[57] Givord D, Rossignol M, Taylor D. Coercivity mechanisms in hard magnetic materials. Journal de Physique IV Colloque. 1992;**02**(C3):95-98

[58] Nikolic VN, Milic MM, Zdravkovic JD, Spasojevic V. Origin of the intrinsic coercivity field variations and magnetic study of ε-Fe₂O₃ phase. Russian Journal of Physical Chemistry A. 2019;**93**(3):588-593

[59] Nikolic VN, Tadic M, Panjan M, Kopanja L, Cvjeticanin N, Spasojevic V. Influence of annealing treatment on magnetic properties of Fe₂O₃/SiO₂ and formation of ε-Fe₂O₃ phase. Ceramics International. 2016;**43**(2):3147-3155

[60] Nikolic VN, Milic MM, Zdravkovic JD, Spasojevic V. Origin of the intrinsic coercivity field variations of ε-Fe₂O₃. Russian Journal of Physical Chemistry A. 2019;**93**(2):377-383

[61] Schmidt H, Asztalos A, Bok F, Voigt W. New iron (III) nitrate hydrates: Fe (NO₃)₃·xH₂O with x= 4, 5 and 6. Acta Crystallographica Section C: Crystal Structure Communications. 2012;**68**(6):29-33

[62] Nikolic VN, Spasojevic V. Analysis of ZFC/FC curves of hematite-silica nanocomposite materials. In: 8th. Belgrade, Serbia: International Conference on Defensive Technologies; 2018

[63] Nikolic VN, Spasojevic V, Panjan M, Kopanja L, Mrakovic A, Tadic M. Re-formation of metastable

ε-Fe$_2$O$_3$ in post-annealing of Fe$_2$O$_3$/ SiO$_2$ nanostructure: Synthesis, computational particle shape analysis in micrographs and magnetic properties. Ceramics International. 2017;**43**(3):7497-7507

[64] Sakurai S, Tomita K, Hashimoto K, Yashiro H, Ohkoshi S. Preparation of the nanowire form of ε-Fe$_2$O$_3$ single crystal and a study of the formation process. Journal of Physical Chemistry C. 2008;**112**(5):20212-20216

[65] Sakurai S, Jin J, Hashimoto K, Okhoshi S. Reorientation phenomenon in a magnetic phase of ε-Fe$_2$O$_3$ Nanocrystal. Journal of the Physical Society of Japan. 2005;**74**(7):1946-1949

[66] Gao H, Yang J. Nanoscale silicon dioxide prepared by sol-gel process. Modern Applied Science. 2010;**4**(9):152-156

[67] Nikolic VN, Tadic M, Mrakovic A, Spasojevic V. Unusual temperature dependence of coercivity in ε-Fe$_2$O$_3$ phase. In: 9th International Conference on Nanomaterials-Research & Application; Brno, Czech. 2017

[68] Tauxe L, Mullender TAT, Pick T. Potbellies, wasp-waists, and superparamagnetism in magnetic hysteresis. Journal of Geophysical Research: Solid Earth. 1996;**101**(B1):571-583

[69] Guo XH, Deng YH, Gu D, Che RC, Zhao DY. Synthesis and microwave absorption of uniform hematite nanoparticles and their core-shell mesoporous silica nanocomposites. Journal of Materials Chemistry. 2009;**19**(2):6706-6712